*Q. J. R. Meteorol. Soc.* (2005), **131**, pp. 1997–2017 doi: 10.1256/qj.04.134

# Parametrization of ice-particle size distributions for mid-latitude stratiform cloud

By P. R. FIELD[1]*, R. J. HOGAN[2], P. R. A. BROWN[1], A. J. ILLINGWORTH[2], T. W. CHOULARTON[3] and R. J. COTTON[1]
[1]*Met Office, UK*
[2]*University of Reading*
[3]*University of Manchester*

(Received 1 September 2004, revised 20 December 2004)

SUMMARY

Particle size distributions measured by the UK C-130 aircraft in ice stratiform cloud around the British Isles are analysed. Probability distribution functions over large scales show that the zeroth, second and fourth moments (equivalent to concentration, ice water content and radar reflectivity) as well as mean particle size have monomodal distributions. Rescaling of the size distributions requiring knowledge of two moments reveals a 'universal' distribution that has been fitted with analytically integrable functions. The existence of the 'universal' distribution implies that two-moment microphysics schemes are adequate to represent particle size distributions (PSDs). In large-scale models it may be difficult to predict two moments, and so power laws between moments have been found as functions of in-cloud temperature. This means that a model capable of predicting ice water content and temperature can predict ice PSDs to use for calculations requiring knowledge of the size distribution (e.g. precipitation rate, radar reflectivity) or to make direct use of the power laws relating moments of the size distribution.

KEYWORDS: Aggregation Aircraft observations

## 1. INTRODUCTION

Knowledge of the shape of the ice-particle size distribution (ice PSD) is crucial for the prediction of processes such as precipitation and radiative effects within large scale models. Accurate PSDs can also be used to predict the radiative and radar properties of clouds. Here, we investigate PSDs of mid-latitude stratiform cloud associated with frontal systems that have been sampled around the British Isles.

Recently, analysis of size distributions has utilized rescaling of the data to identify underlying universal distributions. The rescaling of PSDs is well known within the aggregation community (e.g. Meakin 1992) and rescaling has been applied to raindrop size-distribution data (Sekhon and Srivastava 1971; Willis 1984; Sempere-Torres *et al.* 1998; Illingworth and Blackman 1999; Testud *et al.* 2001; Lee *et al.* 2004). Sempere-Torres *et al.* (1998) attempted to scale drop size distributions with single-moment normalizations, but a lot of scatter in the underlying distribution still remained. Sekhon and Srivastava (1971) and Willis (1984) used two moments to rescale the data, but assumed an underlying functional form to the data. Testud *et al.* (2001) went on to show that drop size distributions could be successfully scaled by normalizing with liquid-water content and mean volume radius without any knowledge of the underlying universal distribution. Finally, Lee *et al.* (2004) have produced a mathematical framework that generalizes the two-moment scaling of drop size distributions using any two moments, and has shown that the results of previous work are special cases within this general scaling approach. Field and Heymsfield (2003) showed that ice-crystal PSDs could be rescaled using precipitation rates and characteristic sizes, and Tinel *et al.* (2005) have recently rescaled ice size distributions by first converting the ice particle sizes to equivalent melted diameters by assuming a mass–size relationship. Westbrook *et al.* (2004a,b)

* Corresponding author: Met Office, FitzRoy Road, Exeter EX1 3PB, UK. e-mail: prfield@ucar.edu

have described a framework for scaling PSDs, and showed that scaling can be applied to ice PSDs obtained in cirrus cloud using two moments of the size distributions without any knowledge of the universal distribution. Westbrook *et al.* have also shown that the universal size distribution is expected to have an exponential tail. These scaling methods show that measured size distributions can be reduced to a single underlying 'universal' size distribution from which the original measured size distribution can be reconstituted given knowledge of two moments. In this work we show that the 'universal' size distribution is applicable for a wide range of ice PSD data, whereas previous work used droplet size distributions. We give best fit curves to the universal distribution that are easily integrable and can be implemented in large-scale models.

Ideally, we would like to reduce the number of moments required to predict the PSD from two to one through the use of power laws that relate one moment to another, as Liu and Illingworth (2000) and Hogan *et al.*[*] have done. In these papers the authors relate radar reflectivity to measured ice water content (IWC) with power laws that vary with in-cloud temperature. Here, we follow a similar procedure but we just use the measured size distributions to generate moments and do not make any assumptions about small-particle contributions or density variations. In this way the user will be able to predict a PSD from the parametrization presented here, and then apply any assumptions they care to make. However, to link these observations to modelling efforts, a mapping from size to mass is required. There is empirical evidence (e.g. Locatelli and Hobbs 1974; Brown and Francis 1995; Heymsfield *et al.* 2004) as well as theoretical evidence from direct simulation of the aggregation process (Westbrook *et al.* 2004a,b) that aggregate ice-crystal mass is proportional to the square of the particle size. In the light of this, we assume that the second moment of the ice-crystal size distribution is proportional to the IWC and use this as our reference moment. Numerous prefactors for the mass–size power law exist and it should be noted that they will vary, based on the properties of the basic monomer crystals that form the larger aggregate. Thus, in this work we investigate the moments of the PSDs so that the minimum number of assumptions about crystal properties are included in the analysis.

In the next section we outline the data and data analysis. In section 3 the observed probability distribution functions of moments of the measured PSDs are presented. Section 4 concerns the correlations between moments, and introduces power laws to relate the second moment of the ice PSD to other moments. Rescaling of the ice PSDs is shown in section 5 and a discussion and conclusions are given in section 6.

## 2. Data analysis

The aircraft data were obtained from flights around the British Isles in cloud (Ns, As, Cs, Ci) associated with mid-latitude cyclonic depressions ('frontal systems'). Table 1 is a list of flights used in this paper. On these flights the clouds were sampled with Particle Measuring Systems (PMS) 2D optical-array probes (2D-C and 2D-P). The 2D-C and 2D-P probes have nominal size ranges of 25–800 and 200–6400 $\mu$m, respectively. The data are split into ten-second segments that have a median length of $\sim$1.2 km, with 90% of the segment sizes in the range 1.0–1.4 km. The data consist of $\sim$9000 $\times$ 10 s ($\sim$1.2 km) segments of in-cloud data (where the 2D probe concentration of super-100 $\mu$m particles greater that one per litre). PSDs that were deemed to consist of raindrops were also eliminated on the basis of shape analysis.

[*] Hogan, R. J., Mittermaier, M. P. and Illingworth, A. J. (2005), paper submitted to the Journal of Applied Meteorology.

TABLE 1. FLIGHT SUMMARY

| Flight | Date | Location around the UK | In-cloud temperature range (°C) |
|---|---|---|---|
| A806 | 21 Nov 2000 | Central England | −23 to +4 |
| A803 | 18 Oct 2000 | South-central England | −32 to +5 |
| A661 | 30 Mar 1999 | South-central England + southern North Sea | −15 to +4 |
| A656 | 8 Mar 1999 | South-west Approaches | −32 to +5 |
| A643 | 8 Dec 1998 | North Sea | − 5 to −2 |
| A639 | 19 Nov 1998 | Bristol Channel | −36 to +5 |
| A627 | 13 Oct 1998 | South-central England | −30 to +10 |
| A606 | 27 Jul 1998 | North Sea | −42 to +3 |
| A290 | 9 Oct 1993 | North Scotland | −50 to −10 |
| A289 | 7 Oct 1993 | North Scotland | −55 to −15 |
| A288 | 6 Oct 1993 | North Scotland | −45 to −5 |
| A287 | 5 Oct 1993 | North Scotland | −50 to −10 |
| A286 | 3 Oct 1993 | North-west Approaches | −50 to −2 |
| A282 | 23 Sep 1993 | North-west Approaches | −30 to −15 |
| A280 | 19 Sep 1993 | Wick | −50 to −10 |
| A279 | 18 Sep 1993 | Scottish Western Isles | −50 to −3 |

Satellite images for these flights are available from www.sat.dundee.ac.uk.

All of the 2D probe data were processed using software supplied by Sky Tech Research Inc. Details about the processing and image recognition algorithms can be found in the paper by Korolev (2003).

Particles were rejected for the following reasons: (i) aspect ratio of the particle $>8$; (ii) particles were too long ($>300$ pixels) in the along-flight direction (due to shedding); (iii) gaps in the image in the along-flight direction; (iv) particles that touched the edge of the array were termed partial and have not been used for this analysis—we decided not to reconstruct partial images because this required some assumptions about the geometry of the particles.

Image recognition was carried out on particles measured by the 2D-C only using the method described by Korolev and Sussman (2000). For complete images that did not touch the edges of the array, a particle needs to occult more than 20 pixels to be classified. Particles that touched the edges (partial images) were classified if they contain more than 180 pixels. This latter classification allows the identification of large dendritic features.

For computation of the size distributions, we have considered only particles that were complete and have used the maximum extent of the particles in the direction parallel to flight. We have repeated the analysis using the particle sizes defined by the perpendicular span and found no significant differences in the results. The ratio of the perpendicular to maximum span for ice-crystal aggregates is expected to be $\sim$0.65 (Westbrook *et al.* 2004a; Korolev and Isaac 2003). Given that the particles are sampled with random orientation, the particle size measured using a single direction to define the size will be, on average, 0.83 of the maximum span.

The combined ten-second size distributions used here have been produced by abutting the bin-width normalized size distributions from the 2D-C (100–475 $\mu$m) and 2D-P (600–4400 $\mu$m). These distributions have then been used to compute moments of the PSDs.

We have ignored particles smaller than 100 $\mu$m, as these are believed to be badly sampled by the 2D-C probe (Strapp *et al.* 2001). We have made no attempt to estimate what the small-particle contribution to the PSD is, as this requires assumptions based on ice-crystal concentration measurements provided by the PMS Forward Scattering Spectrometer Probe, which almost certainly suffers from the effects of ice-particle

shattering on the probe housing that can lead to artificially enhanced concentrations (Field *et al.* 2003).

Occasionally, the large end of the size distribution can exhibit spurious counts in large size-bins due to low sample rates that can adversely skew the computed moments of the distribution. To avoid this problem we have used an upper size limit of 4400 $\mu$m for the computation of moments from the PSDs.

## 3. Observed probability distribution function

We begin by surveying the range of the data presented in this study by considering the PSD moments obtained from the ten-second combined PSDs.

$$\mathcal{M}_n = \int_0^\infty D^n N(D)\,\mathrm{d}D \approx \sum_{D=100\ \mu\mathrm{m}}^{D=4400\ \mu\mathrm{m}} D^n N_D, \tag{1}$$

where $D$ is a particle size parallel to the flight direction, $N(D)\,\mathrm{d}D$ is the concentration of particles with sizes between $D$ and $D + \mathrm{d}D$, $N_D$ is the particle concentration in the size-bin with size $D$, and $n$ is the moment order. The characteristic or mean particle sizes are defined as (following Lee *et al.* 2004).

$$L_{ij} = \left(\frac{\mathcal{M}_j}{\mathcal{M}_i}\right)^{1/(j-i)}, \tag{2}$$

where $i$ and $j$ are the moment orders.

We have plotted histograms of various parameters from different temperature ranges (5C to $-55\,^\circ$C in $10\,^\circ$C intervals). Figures 1–3 show the results for $\mathcal{M}_0$, $\mathcal{M}_2$ and $\mathcal{M}_4$ ($\mathcal{M}_0$ is the concentration for $D > 100$ $\mu$m). Assuming the ice-particle mass is proportional to the square of the particle size means that $\mathcal{M}_2$ is directly proportional to the IWC and, because radar reflectivity for Rayleigh scattering is proportional to mass squared, $\mathcal{M}_4$ is directly proportional to the radar reflectivity ($Z$). It can be seen in these figures that the distributions are generally monomodal, as Hogan and Illingworth (2003) also found when looking at radar data. The mean and standard deviation of the distributions were computed for the moments. The fractional standard deviation (FSD) defined as the quotient of the standard deviation and the mean are given in each figure. The mean and FSD of $\mathcal{M}_0$ (concentration for $D > 100$ $\mu$m) shows no significant variation with temperature, in agreement with observations reported by Korolev *et al.* (2000) and Jeck (1998) that showed similar mean concentrations for super-100 $\mu$m ice particles. This is significant because many ice-nuclei parametrizations have increasing ice-nuclei concentration with decreasing temperature, as discussed by Korolev *et al.* (2000). The inference is that, either the temperature dependence of ice-nuclei concentration over large scales is incorrect, or physical processes (such as diffusional growth, aggregation and secondary ice production) decouple the super-100 $\mu$m particles from the primary nucleation concentrations. The mean of $\mathcal{M}_2$ shows a consistent increase with increasing temperature, but the overall change is still within the spread of the distributions. Again, the FSDs are similar for the distributions at different temperatures. An increase in the mean of $\mathcal{M}_4$ with increasing temperature is more evident, but the natural variability still swamps variations as a function of temperature. The FSDs for this moment show a maximum at $-30\,^\circ$C.

Figures 4 and 5 show histograms of the mean particle size $L_{23}$ (equivalent to mass-weighted mean particle size) and $L_{24}$ (reflectivity-weighted mean size), respectively.

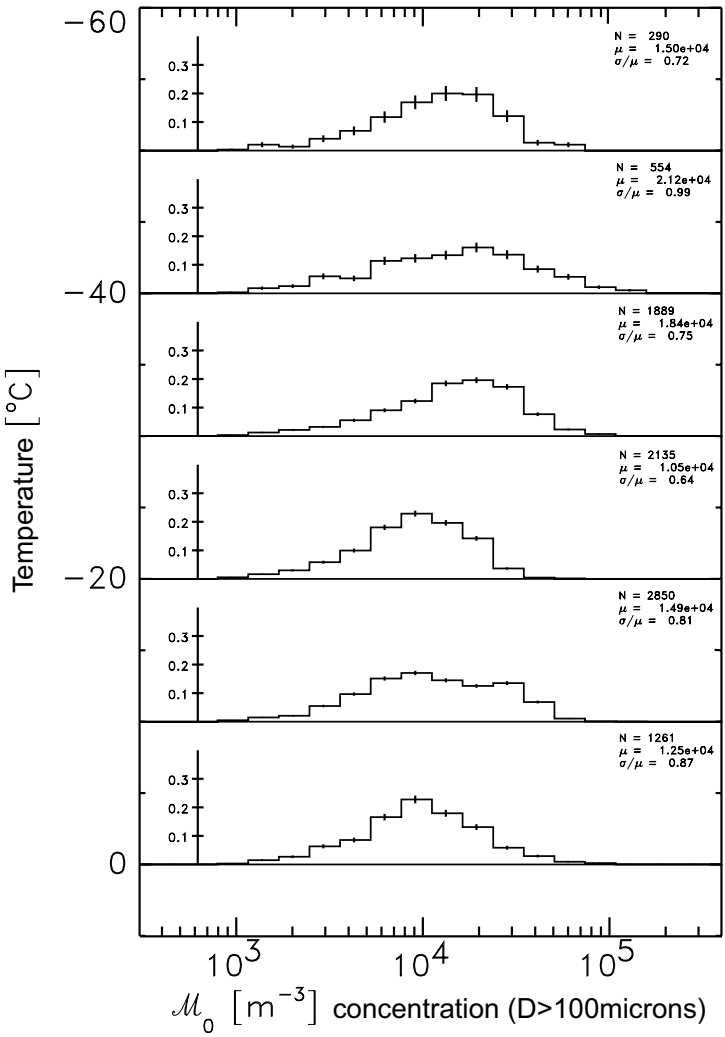


Figure 1. Observed probability distribution functions of the zeroth moment of the particle size distribution, $\mathcal{M}_0$ (concentration for $D > 100$ $\mu$m), for six different temperature ranges (5 °C to –55 °C in 10 °C intervals). The error bars are the Poisson counting error in each bin. The inset vertical axis is the normalized frequency. $N$ is the number of points in the histogram, $\mu$ is the mean, and $\sigma/\mu$ is the fractional standard deviation.

In these figures the mean size shows an increase of a factor ~10 from the coldest to the warmest temperature ranges. The FSDs of the distributions are smaller than the FSDs for the distributions of moments. At the warmest temperatures, the histograms show some skewing towards smaller sizes that are, perhaps, associated with sublimating cloud elements. Also shown in Fig. 4 is the $L_{23}$ estimated from exponential fits to data obtained in the Tropical Rainfall Measurement Mission (TRMM) characterization aircraft campaigns in tropical anvil cloud (Heymsfield *et al.* 2002). Ryan (2000) has also suggested a dependence of mean particle size on temperature, based on examining aircraft observations from stratiform cloud and that is also overplotted in Fig. 4. For an exponential distribution of the form $N(D) = N_0 \exp(-\lambda D)$, the mean particle size is given by $L_{23} = 3/\lambda$. There appears to be good agreement, given the difference in cloud types and environments investigated. The match with the TRMM relationship

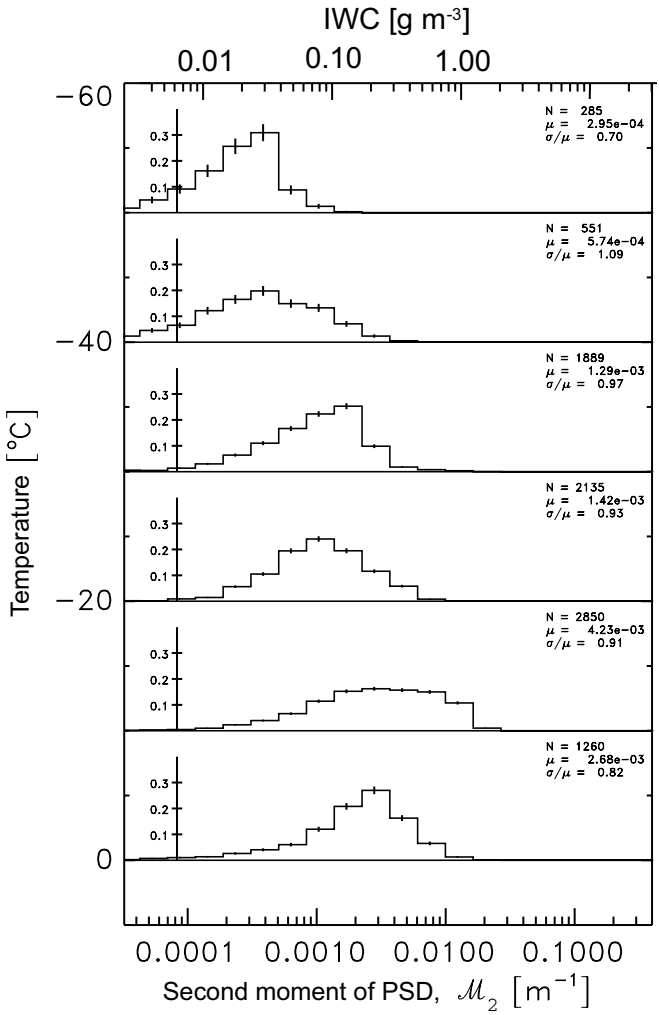


Figure 2. As Fig. 1, but for the second moment of the particle size distribution, $\mathcal{M}_2$ (proportional to ice water content if ice-crystal mass is proportional to size squared). The scale at the top shows the ice water content assuming that ice-crystal mass (kg) $= 0.069 \times \{\text{ice crystal size (m)}\}^2$ (Wilson and Ballard 1999).

is encouraging as it suggests that these observations may be applicable outside of the context of mid-latitude stratiform cloud. Further evidence for a wider applicability of these results is the found in the study of Jeck (1998), which also shows an increase in maximum ice-particle size as function of increasing temperature. The consistent variation of mean size with temperature requires explanation. Although a complete investigation of this relationship is outside the scope of this paper, we suggest that a strong possibility is the dominance of the aggregation process in controlling the evolution of the ice PSD. For aggregation we would expect mean size to be related to depth below cloud top (e.g. Field 2000). But, because frontal clouds have grossly similar height structures, this may mean that, on average, in-cloud temperature is a good proxy for the depth below cloud top, and hence for the time available for aggregation to occur.

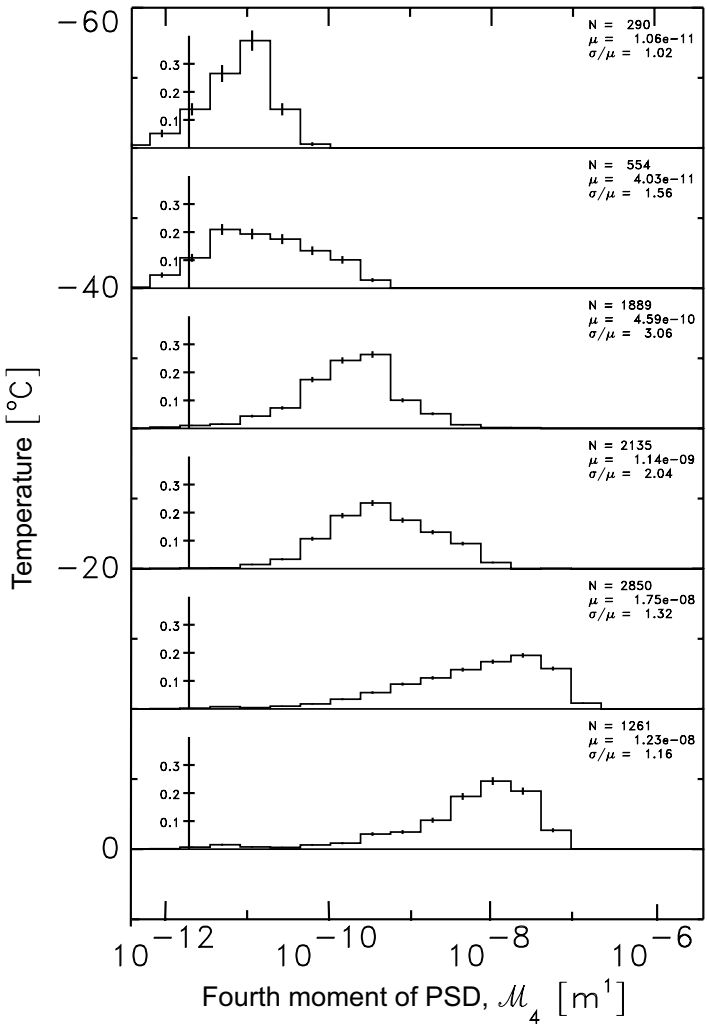


Figure 3. As Fig. 1, but for the fourth moment of the particle size distribution, $\mathcal{M}_4$ (proportional to radar reflectivity for pure Rayleigh scattering if ice-crystal mass is proportional to size squared).

## 4. MOMENT RELATIONS

We now go on to examine correlations between moments. Figures 6(a) and (b) show plots of $\mathcal{M}_2$ against $\mathcal{M}_3$ and $\mathcal{M}_4$. The different shading of the points indicates different temperature intervals (darker shades represent warmer temperatures). Looking at all of the data indicates that simply using $\mathcal{M}_2$ to predict $\mathcal{M}_3$ or $\mathcal{M}_4$ would result in a large amount of scatter. However, if temperature information is used, power laws for different moments of order $n$ can be found for each temperature interval ($T_c$).

$$\mathcal{M}_n = a(n, T_c)\mathcal{M}_2^{b(n,T_c)}. \tag{3}$$

The exponents, $b(n, T_c)$, and coefficients, $a(n, T_c)$, of these power laws vary monotonically and can be related simply to temperature. In order to allow the estimation of a wide range of non-integer moments, we have fitted a two-dimensional polynomial to the power law exponents and coefficients as a function of temperature and moment

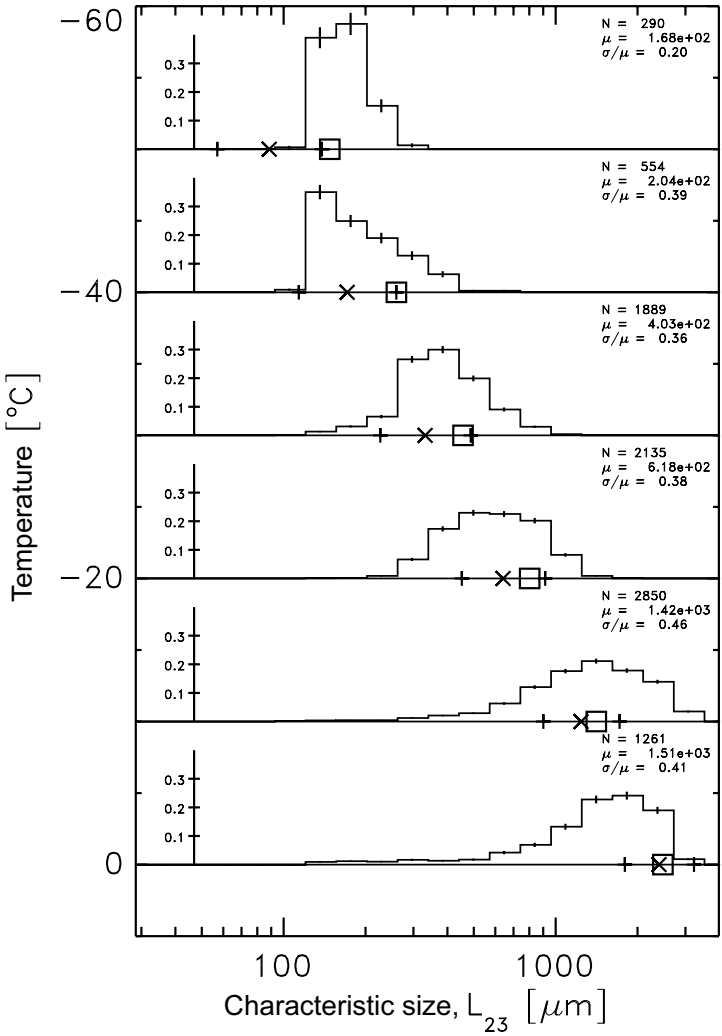


Figure 4. As Fig. 1, but for the characteristic size of the particle size distribution, $L_{23}$. The × symbols and associated error bars along the horizontal axis for each distribution represent estimates of $L_{23}$ obtained from the parametrization of λ from Tropical Rainfall Measuring Mission (TRMM) data (Heymsfield *et al.* 2002). The □ symbols represent the parametrization of λ suggested by Ryan (2000).

order (see Table 2). Figures 7(a) and (b) show the coefficients and the exponents from power laws fitted to integer moments zero to five, and the lines are the fitted polynomial function for the relevant moment orders. It can be seen that the exponent varies with temperature, which contrasts with the results from Lui and Illingworth (2000) and Hogan *et al.* (personal communication) who reported that power laws between IWC and the radar reflectivity $Z$ have a constant exponent. We interpret this difference as arising from the fact that, in this study, we do not introduce any small particles into the PSD for sizes smaller than 100 $\mu$m. The choice of a 100 $\mu$m minimum particle size and 1 $l^{-1}$ minimum concentration leads to a convergence of the moments. If the PSDs were monodisperse we would expect a convergence for $\mathcal{M}_2$ and $\mathcal{M}_4$ at $10^{-5}$ $m^{-1}$ and $10^{-13}$ m, respectively, which is similar to the convergence seen in Fig. 6(b). The addition of a small-particle component to the PSD will have the effect of moving the point at

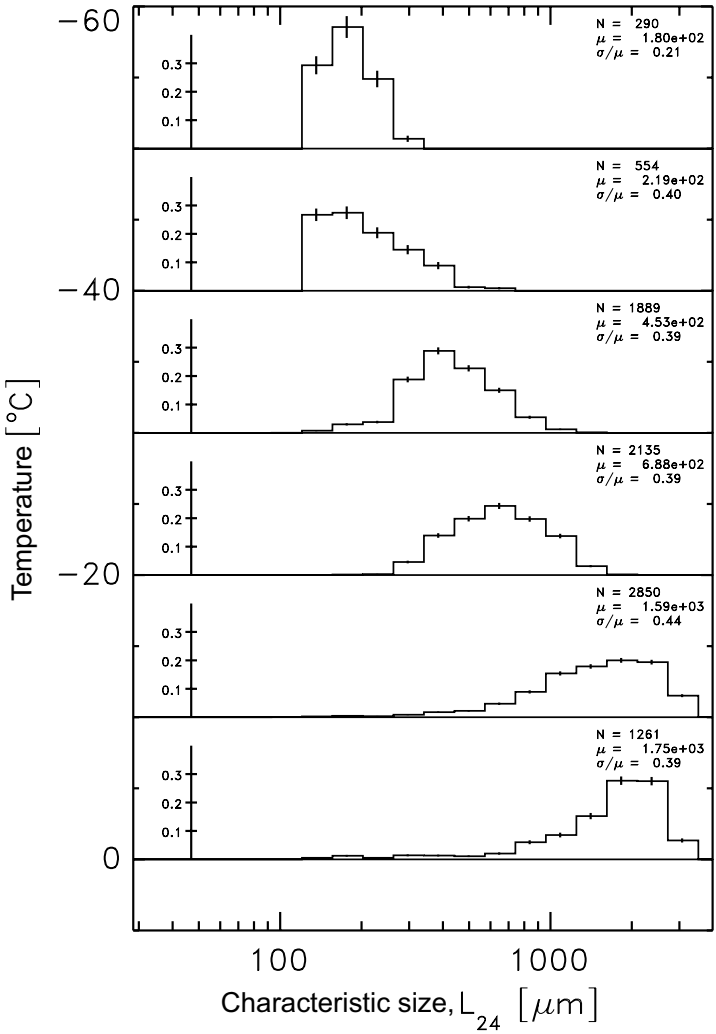


Figure 5. As Fig. 1, but for the characteristic size of the particle size distribution, $L_{24}$.

which the moments converge to much smaller values, depending on the assumptions made, and change the values of the power-law exponents. Our aim here is to reproduce good estimates of measured PSDs, and to this end we believe that, in this case, it is better to introduce no assumptions about the nature of the PSD at sub-100 $\mu$m sizes and accept that a contribution from small particles is neglected. However, we can still gauge the importance of the small-particle contribution and consider it in the discussion. After prediction of the PSDs the user can then subsequently modify the PSD to introduce a more realistic small-particle contribution.

Given the measured value of $\mathcal{M}_2$, the measured temperature and the moment required we can now compare moments derived using the power law with the measured values. Figure 8 shows four comparisons of the measured and derived values of $\mathcal{M}_2$, $\mathcal{M}_3$, $\mathcal{M}_4$, $\mathcal{M}_{2.53}$. The moment of order 2.53 is of interest as it is proportional to the snow precipitation rate in the Met Office numerical weather model (Wilson and Ballard 1999).

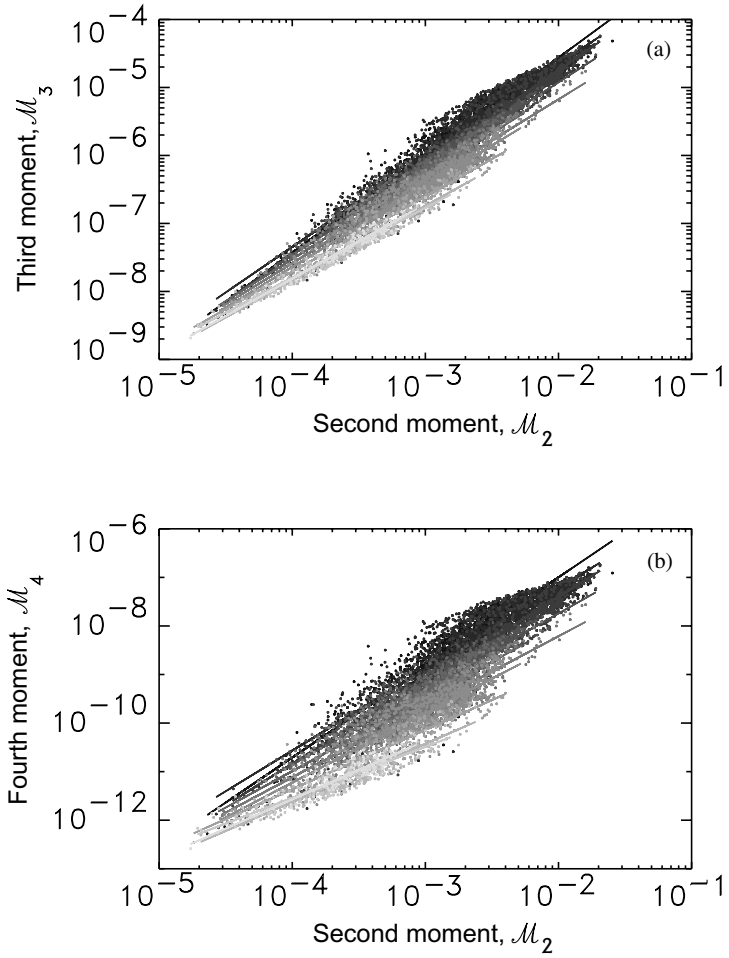


Figure 6. Scatter plots of moments obtained from ∼9000 ten-second particle size distributions (PSDs). The shading represents different temperature intervals. The darker shading represents the warmer temperatures. Best-fit power laws are also shown. (a) The second moment of the PSD, $\mathcal{M}_2$, versus the third moment of the PSD, $\mathcal{M}_3$. (b) The second moment of the PSD, $\mathcal{M}_2$, versus the fourth moment of the PSD, $\mathcal{M}_4$.

It can be seen that the derived moments are in good agreement with the measured ones and that the scatter increases with increasing moment order. We have tested whether our filtering of the data, using a minimum particle size and concentration, will affect the prediction of moments using the power laws derived above, by filtering out PSDs with concentrations 50 times greater than that used in the previous analysis. Although the best-fit lines are slightly different, the previous relations used to predict other moments are still valid and scatter plots of the predicted versus measured moments are merely a subset of those shown in Fig. 8 based on the new filtering applied. Therefore, we are confident that the power laws can be used to predict other moments.

The variability and hence an estimate of the standard deviation of the fractional error (SDFE*) incurred by using the power laws and temperature to estimate the moments is shown in Fig. 9. Figure 9 is similar to the result found by Lee *et al.* (2004) in that the error associated with estimating moments increases with the absolute difference

* Defined as the standard deviation of $(\mathcal{M}_{n,\text{derived}} - \mathcal{M}_{n,\text{measured}})/\mathcal{M}_{n,\text{measured}}$.

TABLE 2. COEFFICIENTS AND EXPONENTS OF MOMENT POWER LAWS $\mathcal{M}_n = a(n, T_c)\mathcal{M}_2^{b(n,T_c)}$ (SI units)

| $x$ | $a_x$ | $b_x$ |
|---|---|---|
| 1 | 5.065339 | 0.476221 |
| 2 | −0.062659 | −0.015896 |
| 3 | −3.032362 | 0.165977 |
| 4 | 0.029469 | 0.007468 |
| 5 | −0.000285 | −0.000141 |
| 6 | 0.312550 | 0.060366 |
| 7 | 0.000204 | 0.000079 |
| 8 | 0.003199 | 0.000594 |
| 9 | 0.000000 | 0.000000 |
| 10 | −0.015952 | −0.003577 |

$n$ = moment order,
$T_c$ = in-cloud temperature (°C),

$$\log_{10} a(n, T_c) = a_1 + a_2 T_c + a_3 n + a_4 T_c n + a_5 T_c^2 + a_6 n^2 + a_7 T_c^2 n + a_8 T_c n^2 + a_9 T_c^3 + a_{10} n^3,$$

$$b(n, T_c) = b_1 + b_2 T_c + b_3 n + b_4 T_c n + b_5 T_c^2 + b_6 n^2 + b_7 T_c^2 n + b_8 T_c n^2 + b_9 T_c^3 + b_{10} n^3.$$

between the order of the reference moment (in this case, two) and the predicted moment. The errors here are a combination of the variability within the PSDs and the polynomial fit used to represent the exponents and coefficients of the power laws. The smallest SDFE of 7% is as expected for $\mathcal{M}_2$ and should, theoretically, be zero if there we no error contribution from the polynomial fit to the power laws. Given accurate estimates of $\mathcal{M}_2$ and in-cloud temperature, the estimate of the precipitation rate given by $\mathcal{M}_{2.53}$ has an SDFE of 25% and radar reflectivity $\mathcal{M}_4$ has an SDFE of 115%. If an estimate of the measured PSD is required, then we can combine the relationships between moments described here with the scalable nature of the ice PSDs that is described in the next section.

## 5. SCALING OF THE PARTICLE SIZE DISTRIBUTION

For aggregating systems, after the initial PSD has evolved enough to 'forget' the starting conditions it will approach a universal shape (see Westbrook *et al.* 2004a,b for more details). The generalized scaling function that can be used to represent the PSD that has evolved during ice-crystal aggregation (and droplet coalescence) was given by Lee *et al.* (2004) for any pair of moments of the PSD.

$$N(D) = \mathcal{M}_i^{(j+1)/(j-i)} \mathcal{M}_j^{(i+1)/(i-j)} \phi_{ij}(x) \tag{4}$$

$$x = D \left( \frac{\mathcal{M}_i}{\mathcal{M}_j} \right)^{1/(j-i)} \tag{5}$$

Where $i$, $j$ can take any value $\geqslant 0$ (must be the same for both Eqs. 4 and 5), and $\phi_{ij}$ is the universal function that is scaled to give the observed PSD. The moments of the distribution are given by

$$\mathcal{M}_n = \mathcal{M}_j^{(n-i)/(j-i)} \mathcal{M}_i^{(j-n)/(j-i)} m_n \tag{6}$$

where $m_n = \int_0^\infty x^n \phi_{ij}(x)\, \mathrm{d}x$ is the $n$th moment of the universal function. It can be seen that, for self consistency, when $n = i$, $j$ then $m_n = 1$. This is a property that the universal function must possess.

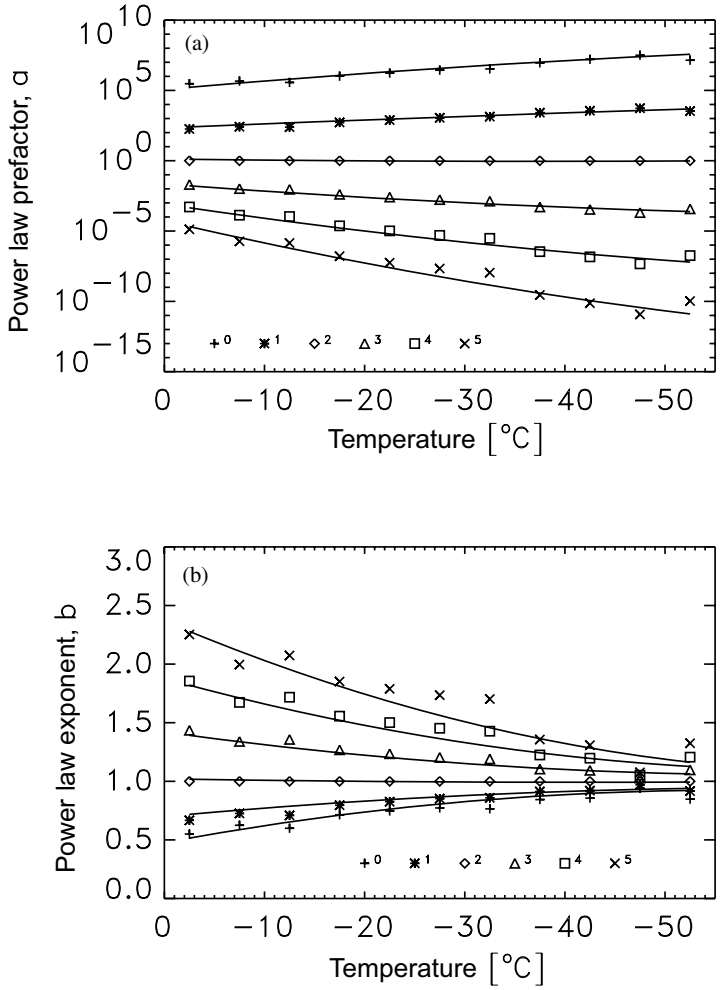


Figure 7. (a) The prefactor, $a$, of the moment-relating power laws, of the form $\mathcal{M}_n = a(n, T_c)\mathcal{M}_2^{b(n,T_c)}$, as a function of temperature for moments of different orders, $n$ (see symbol key). The solid lines represent the solutions of the two-dimensional polynomial fit given in Table 2. (b) The exponent, $b$, of the moment-relating power laws as a function of temperature for moments of different orders. The solid lines represent the solutions of the two-dimensional polynomial fit given in Table 2.

The combination of moments prefixing the universal distribution has previously been termed $N_w$ or $N_0^*$ $(= \mathcal{M}_i^{(j+1)/(j-i)} \mathcal{M}_j^{(i+1)/(i-j)})$ by Illingworth and Blackmann (1999) and Testud *et al.* (2001) for raindrop size distributions, but has recently been used by Tinel *et al.* (2005) to describe ice PSDs. Although it should be noted that Tinel *et al.* first apply a mass–size relationship to convert observed ice-particle size to a melted diameter before rescaling. In Fig. 10(a) we show $N_0^*$ derived using the second and third measured moments as a function of in-cloud temperature. There is an exponential relationship with temperature and a best fit line is shown overplotted ($N_{0,23}^* = 5.65 \times 10^5 \exp(-0.107 T_c)$ m$^{-4}$). In Fig 10(b), histograms of the logarithm of the ratio of measured $N_{0,23}^*$ to that derived by using the temperature relation given above (grey line) and a value derived by predicting the third moment from the measured

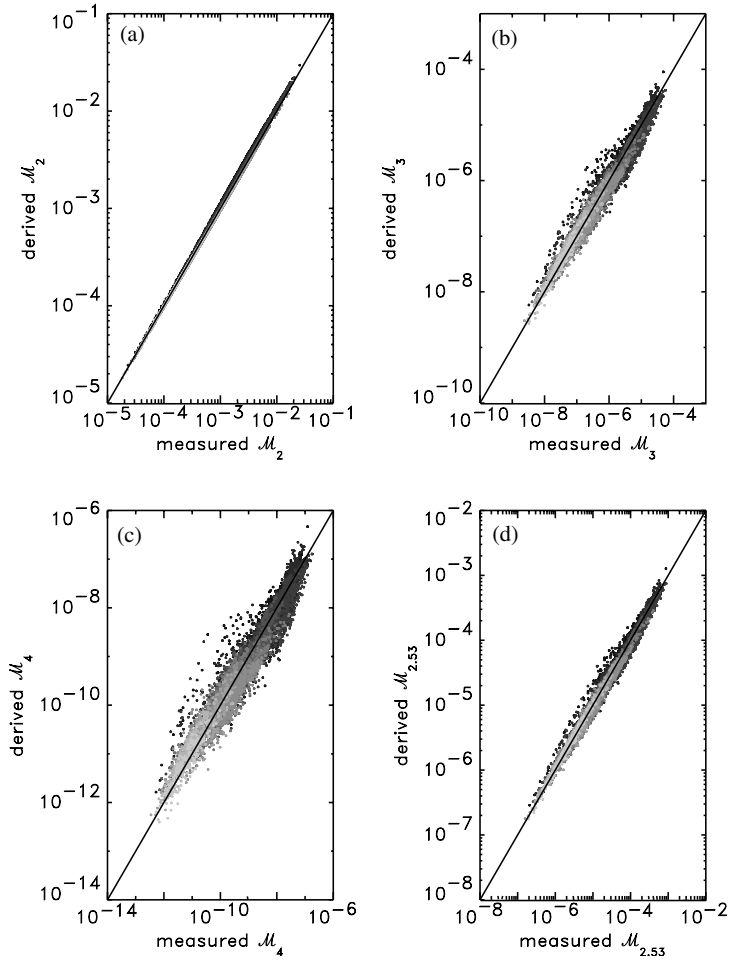


Figure 8. Comparison of measured moments and moments derived using the power-law relations combined with measured values of second moment of the particle size distribution (PSD), $\mathcal{M}_2$, and temperature from ~9000 ten-second PSDs. (a) The second moment of the PSD, $\mathcal{M}_2$; (b) the third moment of the PSD, $\mathcal{M}_3$; (c) the fourth moment of the PSD, $\mathcal{M}_4$; and (d) two-point-five third moment of the PSD—equivalent to precipitation rate in some models, $\mathcal{M}_{2.53}$.

second moment, in-cloud temperature and the moment-relating power laws (black line). It can be seen that there is not much difference between the two methods. However, as an estimate of the third moment is required to convert the dimensionless size to actual particle sizes for the predicted PSD (Eq. (5)), then it is more consistent to use just the moment-relating power laws given in Table 2. An interesting aside is that these two moments can be used to compute $N_0$ for the classic exponential size distribution ($N(D) = N_0 \exp(\lambda D)$), which is simply $N_0 = 13.5 \times N^*_{0,23}$. The current Met Office precipitation scheme (Wilson and Ballard 1999) parametrizes $N_0$ as a function of temperature. These data suggest that the current parametrization is underestimating $N_0$ by about a factor of two.

It can be seen from Eq. (4) that any pair of moments can be used to rescale the data to obtain a universal distribution that does not require any assumptions to be made about the form of the universal distribution. Here, we show the results of rescaling the

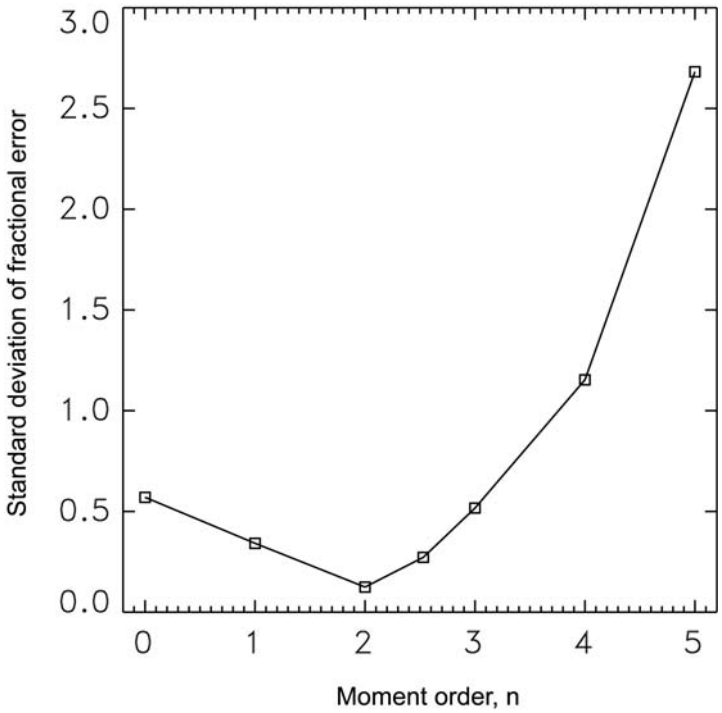


Figure 9. Standard deviation of fractional error (see text) for the derived moment of order, n, obtained from using the measured values of the second moment of the particle size distribution, $\mathcal{M}_2$, and temperature combined with the moment-relating power laws.

~9000 ten-second size distributions for three pairs of moments: ($\mathcal{M}_2$, $\mathcal{M}_3$), ($\mathcal{M}_2$, $\mathcal{M}_4$), and ($\mathcal{M}_3$, $\mathcal{M}_4$) (Fig. 11). Each point in Figs. 11(b), (c) and (d) represents the rescaled contents of a single size bin from the original measured distribution in Fig 10(a).

The universal distributions revealed in Fig. 11 are bimodal, as found by Westbrook *et al.* (2004a,b). The shoulder in the universal distribution is close to $x = 1$ and, hence, this feature in the observed size distributions follows the mass-weighted mean size. For $x \gg 1$ the size distribution appears exponential, as expected (Westbrook *et al.* 2004a,b). For $x < 1$ the size distribution is much steeper. Similar results are obtained if different moments are used from the ones presented here for rescaling the size distributions.

Using these rescaled size distributions, we present fits to each rescaled distribution using a combination of exponential and gamma distributions $\phi_{\mathrm{EG},i,j}(x)$ to represent $\phi_{i,j}$.

$$\phi_{\mathrm{EG},i,j}(x) = \kappa_0 \exp(-\Lambda_0 x) + \kappa_1 x^{\nu} \exp(-\Lambda_1 x), \tag{7}$$

where $\kappa_0$, $\Lambda_0$, $\kappa_1$, $\nu$ and $\Lambda_1$ are the shape parameters. It is shown in the appendix that, because of the self consistency criterion required for the universal distribution, $\kappa_0$ and $\kappa_1$ can be found in terms of the other three shape parameters $\Lambda_0$, $\nu$ and $\Lambda_1$, and so only these three parameters need to be found. We have experimented with generalized gamma functions that only require two shape parameters (e.g. Lee *et al.* 2004) but find that they cannot simultaneously capture both the shoulder feature and the exponential tail of the distribution that theoretical work predicts (Westbrook *et al.* 2004a,b).

To obtain $\Lambda_0$, $\nu$ and $\Lambda_1$ we have chosen many values randomly and select the set that provides the minimum least-squares difference between $\log\{\phi_{\mathrm{EG},i,j}(x)\}$ and the

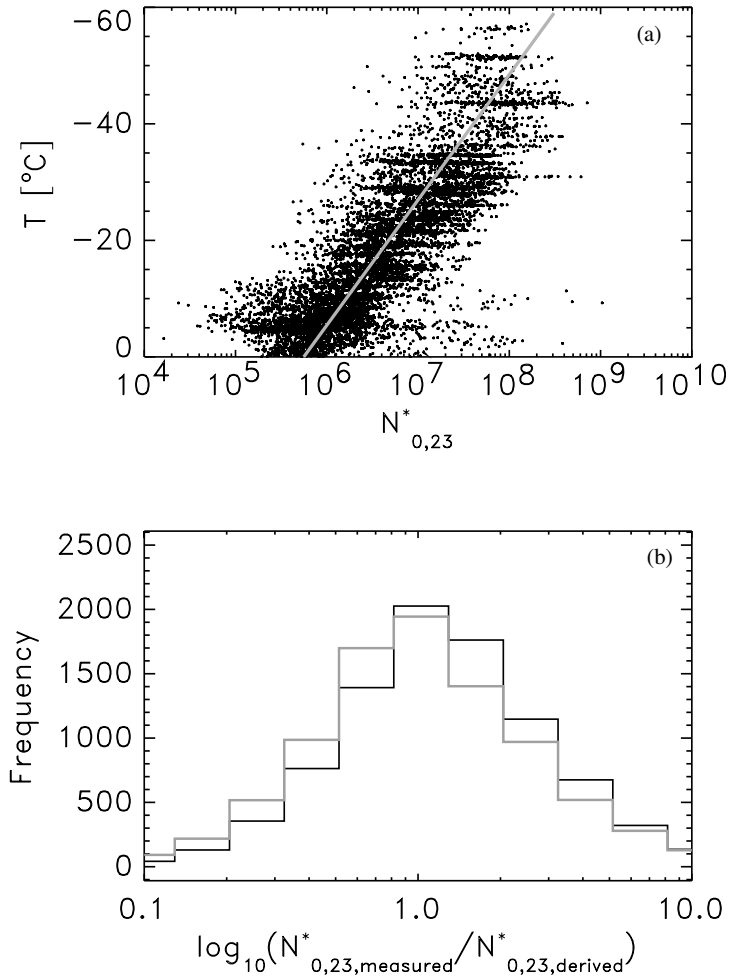


Figure 10. (a) $N^*_{0,23} = \mathcal{M}_2^4 \mathcal{M}_3^{-3}$ computed from measured values for ∼9000 ten-second ice particle size distributions versus in-cloud temperature. The grey solid line is a least-squares fit: $N^*_{0,23} = 5.65 \times 10^5 \exp(-0.107 T_c)$ ($m^{-4}$). (b) Histograms of the logarithm of the ratio of the measured $N^*_{0,23}$ to that derived using the temperature fit shown in (a) (grey line), and to the value derived using a predicted value of $\mathcal{M}_3$ from the measured values of $\mathcal{M}_2$, in-cloud temperature and the moment-relating power-law equations (black line).

logarithm of the rescaled measured PSDs. The results of the fitting exercise are given in Table 3, and the graphical solutions can be seen overplotted in Fig. 11. A fit from Lee *et al.* (2004) to drop size distributions using the third and fourth moments is also shown in Fig. 11(d), and shows good agreement up to $x = 2$ with the fit found here for ice PSDs. For larger sizes the generalized gamma fit decreases more rapidly than the exponential distribution.

We can now test the ability of the universal distribution $\phi_{EG,2,3}$ combined with the power-law relations between moments to reproduce the observed PSDs. We have decided to use the second and third moments in combination with the appropriate universal distribution to predict the PSDs. Using too high or too low a moment would emphasize the small or large end of the PSDs, which are known to be badly sampled by 2D probes due to the probe response time, resolution and sample-volume issues.

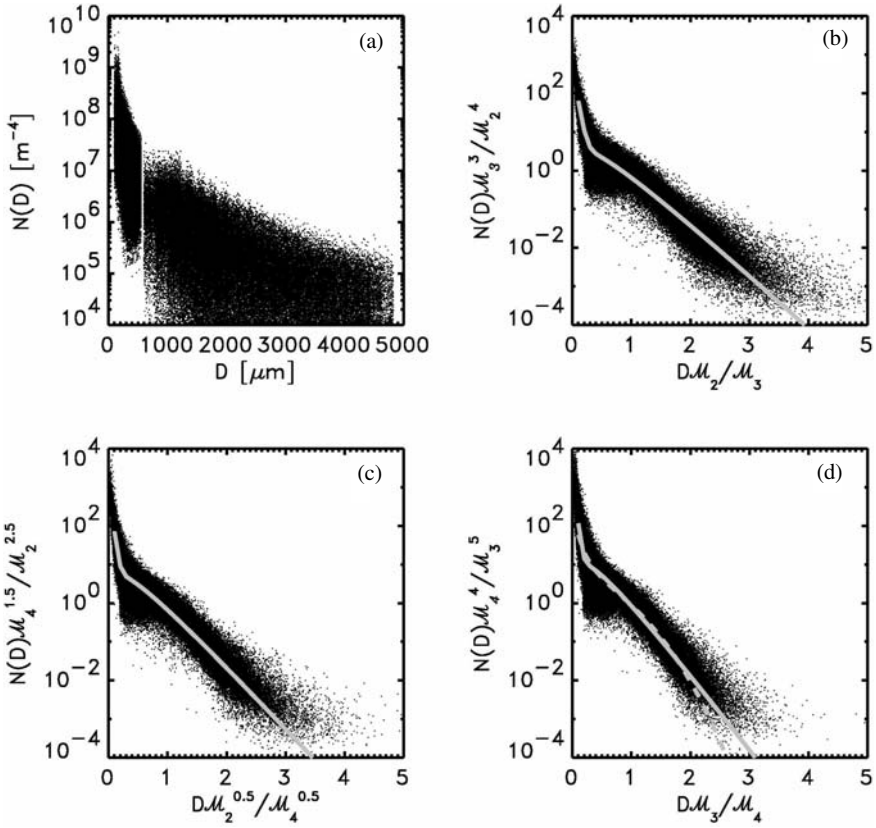


Figure 11. (a) Plot of ∼9000 size distributions used in the analysis. The points represents the bin contents for each ice particle size distribution (PSD). (b) The rescaled PSDs from (a) as a function of dimensionless size using the second moment of the PSD, $\mathcal{M}_2$, and the third moment of the PSD, $\mathcal{M}_3$. The solid line is the combination of exponential and gamma fit. (c) The rescaled PSDs from (a) as a function of dimensionless size using the second moment of the PSD, $\mathcal{M}_2$ and the fourth moment of the PSD, $\mathcal{M}_4$. The solid line is the combination of exponential and gamma fit. (d) The rescaled PSDs from (a) as a function of dimensionless size using the third moment of the PSD, $\mathcal{M}_3$, and the fourth moment of the PSD, $\mathcal{M}_4$. The solid line is a combination of exponential and gamma fit. The dashed line is the generalized gamma function of Lee *et al.* (2004) for raindrop distributions. The functional fits are given in Table 3.

TABLE 3. EXPONENTIAL AND GAMMA FUNCTION FITS TO THE RESCALED SIZE DISTRIBUTIONS

| $i$ | $j$ | $\Lambda_0$ | $\nu$ | $\Lambda_1$ | $\phi_{\mathrm{EG},i,j}(x)$ |
|---|---|---|---|---|---|
| 2 | 3 | 20.78 | 0.6357 | 3.290 | $490.6\exp(-20.78x) + 17.46x^{0.6357}\exp(-3.290x)$ |
| 3 | 4 | 32.78 | 0.8128 | 4.750 | $2837\exp(-32.78x) + 97.95x^{0.8128}\exp(-4.750x)$ |
| 2 | 4 | 29.13 | 0.6496 | 3.909 | $1244\exp(-29.13x) + 33.12x^{0.6496}\exp(-3.909x)$ |

Figure 12 shows some random example distributions selected to show good fits (rows (a) and (b)) defined as those PSDs where the difference between the predicted $\mathcal{M}_3$ and measured $\mathcal{M}_3$ was less than 25%. Mediocre fits are shown in row (c), where the ratio between the predicted $\mathcal{M}_3$ and measured $\mathcal{M}_3$ was ∼2. Bad fits are illustrated in row (d), where the ratio between the predicted $\mathcal{M}_3$ and measured $\mathcal{M}_3$ was ∼5. Using predicted PSDs it is possible to make additional assumptions about the small particle population and recompute the moments if so desired, or to use the PSDs directly in radiation calculations, for example.

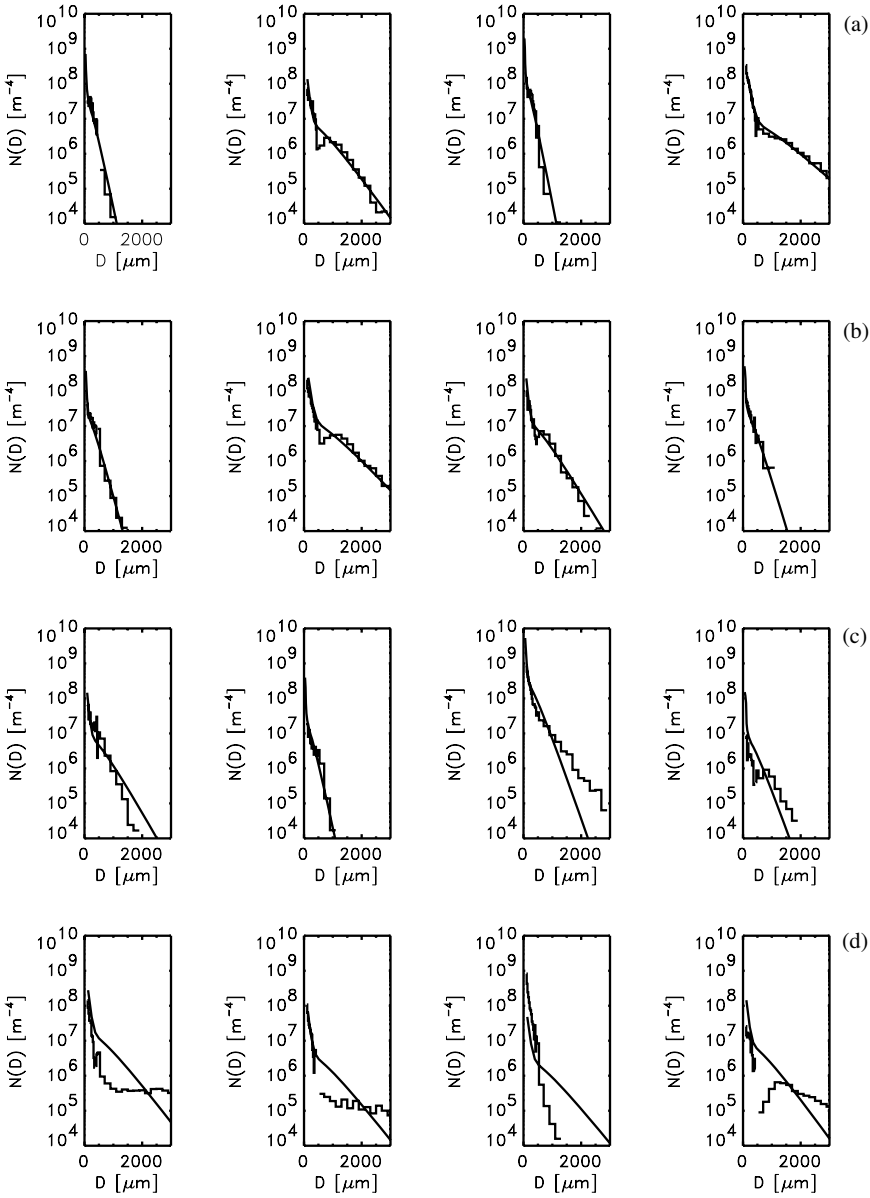


Figure 12. Randomly chosen measured (ten-second average) particle size distributions (PSDs) (stepped line) and PSDs predicted using measured values of the second moment of the PSD, $\mathcal{M}_2$, and temperature to estimate the third moment of the PSD, $\mathcal{M}_3$, combined with the exponential + the gamma fit to the universal distribution given in Table 3 for $\phi_{\mathrm{EG},2,3}$: (a) and (b) good fits, (c) mediocre fits, and (d) bad fits.

## 6. Discussion and conclusions

It has been shown that ice PSDs can be accurately described using knowledge of two moments and the scalable universal distribution only. No assumptions relating particle size to mass are required. Numerical weather prediction models commonly only predict one moment, and so we require a method of estimating a second moment. We have demonstrated that using temperature we can obtain power laws to link a

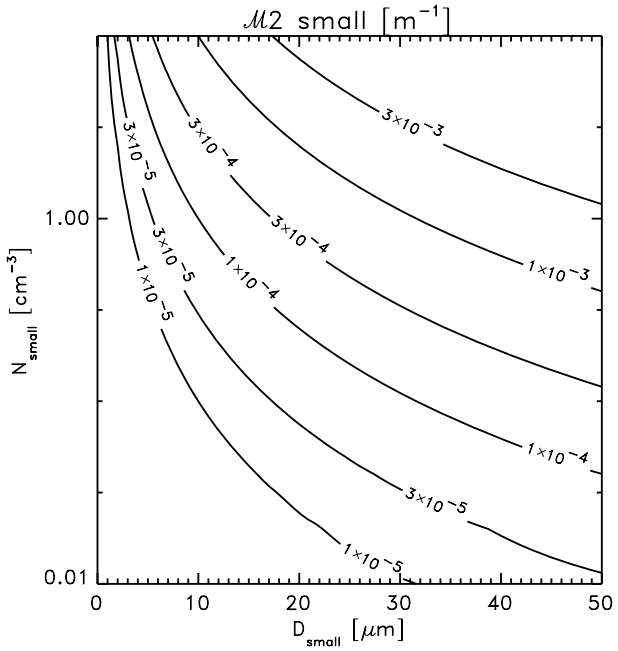


Figure 13. Contribution to the second moment of the particle size distribution, $\mathcal{M}_2$, from small particles represented by a monodisperse distribution with size $D_{\text{small}}$ and concentration $N_{\text{small}}$.

reference moment, in this case the second-order moment, to any arbitrary moment. Thus, moments representing snowfall rate can be directly predicted from the known reference moment and temperature. This approach has the advantage that the shape of the ice PSDs are inherent in the power laws relating the moments. Alternatively, ice PSDs can be predicted and used in radiation codes, or assumptions about the small-particle population or other particle properties can be applied.

The small-particle component of ice PSDs is subject to uncertainty and in this analysis we have decided to ignore the contribution from particles smaller than 100 $\mu$m. However, we can still attempt to gauge whether these small particles will be important by looking at the contribution to $\mathcal{M}_2$ that a monodisperse distribution of small particles would make. In Fig. 13 a contour plot of the contribution to the second moment from small particles is given as a function of small-particle size and small-particle concentration. From Fig. 2 the contribution from small particles would become important if it exceeded $3 \times 10^{-4}$ m$^{-1}$. It can be seen that, to reach this level, the small particles would have to be dominated by 50 $\mu$m particles at concentrations of 0.1 cm$^{-3}$, or by 20 $\mu$m particles with concentrations of 1 cm$^{-3}$. We would maintain that the contribution from small particles to the second moment will only become important where size distributions are narrow, which from these data appears to be at colder temperatures ($T < -40\,^{\circ}$C).

While, in this study, we have dealt with ice PSDs, it is interesting to note that the universal distributions found for drop size distributions show a good match to the rescaled ice PSDs if we use the same moments to scale the data. The agreement of the other overplotted function in Fig. 10(d) of Lee *et al.* (2004) suggests that it may be possible ultimately to treat the ice and raindrop populations with the same approach. We suggest that the similarity between the universal distribution found for

the ice PSDs and the drop size distributions results from the dominant physical process in the evolution of the size distributions: aggregation and coalescence (e.g. Cardwell *et al.* 2002, 2003; Field and Heymsfield 2003; Westbrook *et al.* 2004a,b). For both ice crystals and droplets the collection kernel is controlled by differential sedimentation. It is this similarity in the form of the collection kernel that leads to the same universal distribution.

The use of temperature to predict another moment, given knowledge of one, may be useful for mid-latitude weather prediction, but may not be a completely satisfactory solution globally or for climate prediction. It remains to be seen whether these power laws will hold for the tropics or convective clouds—however, as pointed out earlier it is encouraging that the TRMM data appear to agree in terms of characteristic size as a function of temperature.

We have examined aircraft-mounted 2D probe data from flights carried out in frontal cloud around the British Isles. Analysis of the moments of the ∼9000 ten-second size distributions, and the PSDs themselves, revealed the following:

- Probability distribution functions of ice PSD moments $\mathcal{M}_{0,2,4}$ and characteristic size ($L_{23}$, $L_{24}$) display monomodal distributions. The spread in characteristic sizes is smaller than that seen for individual moments.
- The concentration of particles larger than 100 $\mu$m is independent of in-cloud temperature over large scales.
- There is a correlation between characteristic size ($L_{23}$, $L_{24}$) and temperature. This correlation results in the series of temperature-dependent power laws relating moments. One possible explanation for the good correlation is the action of aggregation as particles fall from colder to warmer temperatures.
- Power-law relations between moments of order $n$ and the second moment as a function of temperature have been found. It is possible to combine measured temperature and a measurement of the second moment of a PSD to obtain another moment, such as precipitation rate, for use in numerical weather-prediction models. In addition, PSDs can be estimated from knowledge of the second moment and in-cloud temperature.
- The observed ice PSDs have been rescaled using two moments of the size distribution to reveal a universal distribution. No assumptions needed to be made about the conversion of particle size to mass to obtain this result.
- The successful rescaling of the size distributions suggest that two-moment schemes can adequately represent ice and raindrop size distributions in mid-latitude stratiform clouds sampled around the UK. We have fitted analytically integrable functions to the rescaled size distributions to represent the universal distributions.

## ACKNOWLEDGEMENTS

The authors wishes to thank the staff of the Meteorological Research Flight and the Royal Air Force C-130 aircrew for their assistance and hard work. This work was partly supported by the Natural Environment Research Council's thematic programme 'Clouds, water vapour and climate'.

## APPENDIX

In this appendix we reduce the number of shape parameters required for the combination of exponential and gamma distributions from five to three by making use of the self consistency constraint. The form of the combined exponential gamma

distribution that will be used to model the universal distribution after rescaling with moments of order $i$ and $j$ is

$$\phi_{\mathrm{EG},i,j}(x) = \kappa_0 \exp(-\Lambda_0 x) + \kappa_1 x^{\nu} \exp(-\Lambda_1 x), \tag{A.1}$$

and the moments of this function are given by

$$m_n = \int_0^{\infty} x^n \phi_{\mathrm{EG},i,j}(x)\, \mathrm{d}x \tag{A.2}$$

$$m_n = \frac{\kappa_0 \Gamma(n+1)}{\Lambda_0^{n+1}} + \frac{\kappa_1 \Gamma(n+\nu+1)}{\Lambda_1^{(n+\nu+1)}}. \tag{A.3}$$

For self consistency we require

$$m_i = m_j = 1, \tag{A.4}$$

and so substituting $i,\ j$ into Eq. (A.3), and rearranging we can find $\kappa_1$:

$$\kappa_1 = \kappa_0 \frac{\dfrac{\Gamma(i+1)}{\Lambda_0^{i+1}} - \dfrac{\Gamma(j+1)}{\Lambda_0^{j+1}}}{\dfrac{\Gamma(j+\nu+1)}{\Lambda_1^{j+\nu+1}} - \dfrac{\Gamma(i+\nu+1)}{\Lambda_1^{i+\nu+1}}}. \tag{A.5}$$

By substituting Eq. (A.5) into (A.3), and letting $m_i = 1$, we obtain $\kappa_0$:

$$\kappa_0 = \frac{1}{\dfrac{\Gamma(i+1)}{\Lambda_0^{i+1}} + \dfrac{\Gamma(i+\nu+1)}{\Lambda_1^{i+\nu+1}} \left\{ \dfrac{\dfrac{\Gamma(i+1)}{\Lambda_0^{i+1}} - \dfrac{\Gamma(j+1)}{\Lambda_0^{j+1}}}{\dfrac{\Gamma(j+\nu+1)}{\Lambda_1^{j+\nu+1}} - \dfrac{\Gamma(i+\nu+1)}{\Lambda_1^{i+\nu+1}}} \right\}}. \tag{A.6}$$

Thus $\phi_{\mathrm{EG},i,j}$ is a function of three shape parameters only: $\Lambda_0$, $\nu$ and $\Lambda_1$.

## References


Brown, P. R. A. and Francis, P. N. 1995 Improved measurements of the ice water-content in cirrus using a total-water probe. *J. Atmos. Ocean. Tech.*, **12,** 410–414

Cardwell, J. R., Choularton, T. W., Wilson, D. R. and Kershaw, R. 2002 Use of an explicit model of the microphysics of precipitating stratiform cloud to validate a bulk microphysics scheme. *Q. J. R. Meteorol. Soc.*, **128,** 573–592

Cardwell, J. R., Field, P. R. and Choularton, T. W. 2003 A modelling study of ice-spectrum modes in deep frontal clouds. *Q. J. R. Meteorol. Soc.*, **129,** 1873–1890

Field, P. R. 2000 Bimodal ice spectra in frontal clouds. *Q. J. R. Meteorol. Soc.*, **126,** 379–392

Field, P. R. and Heymsfield, A. J. 2003 Aggregation and scaling of ice crystal size distributions. *J. Atmos. Sci.*, **60,** 544–560

Field, P. R., Wood, R., Brown, P. R. A., Kaye, P. H., Hirst, E., Greenaway, R. and Smith, R. A. 2003 Ice particle interarrival times measured with a fast FSSP. *J. Atmos. Ocean. Technol.*, **20,** 249–261

Heymsfield, A. J., Bansemer, A., Field, P. R., Durden, S. L, Stith, J. L., Dye, J. E., Hall, W. and Grainger, C. A. 2002 Observations and parameterizations of particle size distributions in deep tropical cirrus and stratiform precipitating clouds: Results from in situ observations in TRMM field campaigns. *J. Atmos. Sci.*, **59,** 3457–3491

Heymsfield, A. J., Bansemer, A., Schmitt, C., Twohy, C. and Poellot, M. 2004 Effective ice particle densities derived from aircraft data. *J. Atmos. Sci.*, **61,** 982–1003

Hogan, R. J. and Illingworth, A. J. 2003 Parameterizing ice cloud inhomogeneity and the overlap of inhomogeneities using cloud radar data. *J. Atmos. Sci.*, **60,** 756–767

Illingworth, A. J. and Blackman, T. M. 1999 'The need to normalize RSDs based on the gamma RSD formulations and implications for interpreting polarimetric radar data'. Pp. 629–631 in Preprint of the proceedings of the 29th International conference on radar meteorology, Montreal, Quebec, Canada

Jeck, R. K. 1998 'Snow and ice particle sizes and concentrations at altitudes up to 9 km (30000 ft)'. Final Report DOT/FAA/AR/97/66, Flight Safety Research Section, Federal Aviation Administration, Office of Aviation Research, Springfield VA, USA

Korolev A. V. 2003 *2D processing software*. Sky Technology Research Inc. (www.skytechresearch.com)

Korolev, A. V. and Isaac, G. 2003 Roundness and aspect ratio of particles in ice clouds. *J. Atmos. Sci.*, **60,** 1795–1808

Korolev, A. and Sussman, B. 2000 A technique for habit classification of cloud particles. *J. Atmos. Ocean. Technol.*, **17,** 1048–1057

Korolev A., Isaac, G. A. and Hallett J. 2000 Ice particle habits in stratiform cloud. *Q. J. R. Meteorol. Soc.*, **126,** 2873–2902

Lee, G., Zawadzki, I., Szyrmer, W., Sempere-Torres, D. and Uijlenhoet, R. 2004 A general approach to double-moment normalization of drop size distributions. *J. Appl. Meteorol.*, **43,** 264–281

Liu, C. L. and Illingworth, A. J. 2000 Toward more accurate retrievals of ice water content from radar measurements of clouds. *J. Appl. Meteorol.*, **39,** 1130–1146

Locatelli, J. D. and Hobbs, P. V. 1974 Fall speeds and masses of solid precipitation particles. *J. Geophys. Res.*, **98,** 8639–8664

Meakin, P. 1992 Aggregation kinetics. *Physica Scripta*, **46,** 295–331

Ryan B. F. 2000. A bulk parameterization of the ice particle size distribution and the optical properties in ice clouds. *J. Atmos. Sci.*, **57,** 1436–1451

Sekhon, R. S. and Srivastava, R. C. 1971 Doppler radar observations of drop-size distributions in a thunderstorm. *J. Atmos. Sci.*, **28,** 983–994

Sempere-Torres, D., Porra, J. M. and Creutin, J. D. 1998 Experimental evidence of a general description for raindrop size distribution properties. *J. Geophys. Res.–Atmos.*, **103(D2),** 1785–1797

Strapp, J. W., Albers, F., Reuter, A., Korolev, A. V., Maixner, U., Rashke, E. and Vukovic, Z. 2001 Laboratory measurements of the response of a PMS OAP-2DC. *J. Atmos. Ocean. Technol.*, **18,** 1150–1170

Testud, J., Oury, S., Black, R. A., Amayenc, P. and Dou, X. K. 2001 The concept of 'normalized' distribution to describe raindrop spectra: A tool for cloud physics and cloud remote sensing. *J. Appl. Meteorol.*, **40,** 1118–1140

Tinel, C., Testud, J., Hogan, R. J., Protat, A., Delanoe, J. and Bouniol, D. 2005 The retrieval of ice cloud properties from cloud radar and lidar synergy. *J. Appl. Meteorol.* (in press)

Westbrook, C. D., Ball, R. C, Field, P. R. and Heymsfield, A. J. 2004a Universality in snowflake formation. *Geophys. Res. Lett.*, doi: 10.1029/2004/GL020363

2004b A theory of growth by differential sedimentation, with application to snowflake formation. *Phys. Rev. E*, **70,** 021403-1–021403-7

Willis, P. T. 1984 Functional fits to some observed drop size distributions and the parameterization of rain. *J. Atmos. Sci.*, **41,** 1648–1661

Wilson, D. R. and Ballard, S. P. 1999 A microphysically based precipitation scheme for the UK Meteorological Office Unified Model. *Q. J. R. Meteorol. Soc.*, **125,** 1607–1636